

THE LkH α 101 INFRARED CLUSTER

M. BARSONY

Department of Astronomy, University of California, Berkeley, and Harvard-Smithsonian Center for Astrophysics, MS-78,
 60 Garden Street, Cambridge, MA 02138¹

J. M. SCHOMBERT²

Department of Astronomy, University of Michigan, Dennison Building, Ann Arbor, MI 48109

AND

K. KIS-HALAS

Department of Astronomy, University of California, Berkeley, CA 94720

Received 1991 February 1; accepted 1991 April 2

ABSTRACT

An $8' \times 12'$ area, corresponding to a 1.9×2.8 pc field centered on the Herbig Ae/Be star, LkH α 101, has been mapped in the near-infrared J and K (1.2 and 2.2 μm) bandpasses at $1''.35 \text{ pixel}^{-1}$ resolution using IRIM on the KPNO 1.3 m telescope. We report the discovery of an embedded cluster of more than 100 young stellar objects within this area. We estimate our completeness limits to be 16.5 mag at J and 14.5 mag at K , although sources as faint as $K = 16.0$ and $J = 17.5$ were detected. We have identified four types of cluster members, defined by their location in the K versus $J-K$ color magnitude diagram: (1) accreting protostars (the Class I sources of Lada and Wilking, which are the sources with $J-K > 4$), (2) probable accreting protostars (sources with $3 < J-K < 4$), (3) embedded, low-mass, pre-main-sequence (PMS) stars younger than 10^6 yr (sources with $K < 13.4$ and $2 < J-K < 3$), and (4) young ($\approx 10^6$ yr), embedded, brown dwarf candidates (sources with $K > 13.4$ and $2 < J-K < 3$). According to this classification scheme, the embedded cluster population of the LkH α 101 cloud core consists of 16 Class I sources, 39 probable Class I sources, 40 young, embedded, low-mass, PMS stars, and 46 young, embedded, brown dwarf candidates. Only eight of the latter have J counterparts. From the relative numbers of sources of each type, we estimate an upper limit for the accreting protostar phase of 4×10^5 yr.

The spatial distribution of the sources in the cloud core is highly nonuniform, such that the youngest sources are the most centrally concentrated. In keeping with this trend, it appears that the most massive star of the cluster, LkH α 101, is probably the youngest. There is also a hint of mass segregation in the cluster, such that $\approx 58\%$ of the brown dwarf candidate sources are concentrated in 17% of the observed area. The star formation efficiency (SFE) in the central $2' \times 2'$ of this cluster is $\approx 18\%$. In the densest parts of the cluster, the observed stellar density places a limit of 1 star per $\approx (2.7 \times 10^{17} \text{ cm}^3)^3$ for the initial volume of gas which can eventually form a star. This volume corresponds to initial masses of 0.045, 0.45, and $4.5 M_{\odot}$ for uniform densities of $\rho_{\text{H}_2} = 10^3, 10^4,$ and 10^5 cm^{-3} , respectively. We find an upper limit of 4×10^5 yr for the protostellar collapse phase in this cluster and infall rates of $1.1 \times 10^{-7}, 1.1 \times 10^{-6},$ and $1.1 \times 10^{-5} M_{\odot} \text{ yr}^{-1}$, corresponding to the above-quoted stellar masses if the collapse time is assumed independent of the final stellar mass.

Subject headings: clusters: open — infrared: sources — stars: Be — stars: brown dwarfs — stars: individual (LkH α 101) — stars: pre-main-sequence

1. INTRODUCTION

LkH α 101 is a bright Herbig Ae/Be star which is the source of a powerful ionized stellar wind, an extended radio H II region, and a reflection nebulosity at a distance of 800 pc (Cohen, Bieging, & Schwartz 1982; Herbig 1971). The recent detection of nearly two dozen new sources at 8000 \AA in a 2.5×4.0 field centered on LkH α 101 (Barsony et al. 1990) prompted further investigation of this source at near-infrared wavelengths. The discovery of a radio star cluster around LkH α 101 (Becker & White 1988) provided another clue to the possible existence of an embedded pre-main-sequence population in this source, since the preponderance of radio-emitting

sources among pre-main-sequence stars is now well established (André, Montmerle, & Feigelson 1987; André et al. 1988; Montmerle & André 1988; Stine et al. 1988; Leous et al. 1991).

The question of exactly how clouds collapse to form stars is still open. Do stars form in isolation or in clusters? In the Taurus and Perseus clouds, for example, the dominant model of star formation seems to be the former: that is, one or two sources form per cloud core (Beichmann et al. 1986; Kenyon et al. 1990; Myers 1990, private communication). However, in other regions, such as ρ Oph (Barsony et al. 1989; Wilking, Lada, & Young 1989) and Orion (Lada et al. 1991; McCaughrean 1989) spatially concentrated associations of stars form together.

Perhaps the most glaring unanswered question in star formation studies is still why all the available gas in a cloud core does not get used up to form stars. The ratio of $M_{\text{stars}}/M_{\text{total}}$ in

¹ Current postal address.

² Visiting Astronomer, Kitt Peak National Observatory, National Optical Astronomy Observatories, operated by AURA, Inc., under contract with the National Science Foundation.

a star-forming region can vary from a few percent to 42% (Lada & Lada 1991), depending upon the source in question and upon the size of the region under consideration. Precise values for star formation efficiencies are constantly being revised with the availability of new IR array camera data and new molecular line maps of star-forming clouds, but there is no known case in which all the available gas has been converted to stars. What determines star formation efficiency?

It is also not clear what determines the initial conditions for star formation. What determines the volume of gas from which a star will collapse? How does this volume vary from star to star? It seems natural to conjecture that massive stars must collapse from larger volumes than less massive stars. Following this line of reasoning, one would assume the stellar IMF to be related to the cloud clump mass spectrum, with the more massive stars forming from more massive clumps.

Data are just becoming available on cloud clump mass spectra (i.e., plots of $\log_{10} dN/dm$ versus $\log_{10} m$, with dN/dm in units of number of stars per unit solar mass bin, and m in units of M_{\odot}). Preliminary results show a cloud clump mass spectrum going as $M_{\text{clump}}^{-1.6}$ for $10 M_{\odot} < M_{\text{clump}} < 1000 M_{\odot}$ in M17 (Stutzki & Güsten 1990), and as $M_{\text{clump}}^{-1.6}$ for $M_{\text{clump}} > 30 M_{\odot}$ in Orion (Lada et al. 1991). For ρ Oph, the cloud clump mass spectrum goes as $M_{\text{clump}}^{-1.1}$ for the mass range $10 M_{\odot} < M_{\text{clump}} < 844 M_{\odot}$ (Loren 1989). The clump mass spectrum turns over for lower masses in both ρ Oph (for $M_{\text{clump}} < 10 M_{\odot}$) and Orion (for $M_{\text{clump}} < 30 M_{\odot}$), although both authors cite incompleteness at lower masses as the explanation. Recall that the stellar mass function ($\log_{10} dN$ vs. $d \log_{10} m$) goes as $M_{\text{star}}^{-1.35}$ for $0.4 M_{\odot} < M_{\text{star}} < 10 M_{\odot}$ (Salpeter 1955).

When we try to relate cloud clump mass spectra to stellar mass spectra, at least two important considerations must be taken into account. First, we have yet to fully explore the clump mass spectrum for masses below $10 M_{\odot}$, as pointed out above, but this is precisely the mass range which is interesting in the context of stellar masses. Second, only the mass spectra of virialized clumps could possibly be relevant to the stellar mass function, since unvirialized clumps will never form stars (Myers 1990, private communication). However, most cloud clumps in ρ Oph are thought to be unvirialized (Loren 1989).

Another intriguing question relates to differences in the formation mechanisms between ordinary and massive ($\geq 8 M_{\odot}$) stars: Do all massive stars form in clusters, or can they, too, form in isolation? The evidence to date seems to favor the idea that massive stars preferentially form in star clusters (Blaauw 1964; Larson 1990; Zinnecker 1990), often near the geometric center of the related stellar association. However, a systematic investigation of an unbiased sample of high-mass star-forming regions with infrared arrays is called for to give a conclusive answer to this question.

In this paper, we report the discovery of a new embedded young star cluster (consisting of more than 100 sources) surrounding LkH α 101. We describe the criteria used to identify cluster members, and further criteria by which the nature of the embedded population was determined. We demonstrate the spatial segregation of the embedded population according to age and mass and derive the maximum infall radius at the cluster center from the constraint provided by the observed stellar density. By comparing our data with reddened main-sequence, pre-main-sequence, and brown dwarf evolutionary tracks, we can estimate the cluster age, which agrees well with the upper limit on the cluster age derived from kinematic considerations. From the observed numbers of sources in different

evolutionary states, we derive an upper limit to the time a star spends in the protostar phase in this cluster. We also estimate the star formation efficiency in the central $2' \times 2'$ area.

We describe our observations and data reduction methods in § 2. Our results are presented in § 3 and are further discussed in § 4. Our conclusions are summarized in § 5.

2. OBSERVATIONS AND DATA REDUCTION

The LkH α 101 region was observed on the nights of 1990 March 13–15 at the KPNO 1.3 m telescope. The detector was 58×62 InSb array with $1''.35$ pixels (Fowler et al. 1987). Six grids, each consisting of 4×4 frames, were mapped through the J ($\lambda = 1.25 \mu\text{m}$, $\delta\lambda = 0.27 \mu\text{m}$) and K ($\lambda = 2.16 \mu\text{m}$, $\delta\lambda = 0.38 \mu\text{m}$) filters. The frames were overlapped by $15''$ in right ascension and declination to make subsequent mosaicing of the frames feasible. The integration time was 60 s per frame resulting in a nominal sensitivity limit of ≈ 17 mag at J and ≈ 15.5 at K . Telescope drift was monitored between each grid by offsetting to a nearby bright infrared source and was always found to be less than $15''$.

Infrared standard stars (Elias et al. 1982) were observed at the beginning, middle, and end of each night to cover various air masses and colors. Star exposures were taken out of focus so that the brightest pixels did not register more than 10,000–15,000 ADU to keep the detector response in the linear regime. Four snaps in each filter were taken of each standard star; one in the center and three in each corner of the chip to correct for responsivity variations across the chip. Short dark exposures were taken after each standard observation.

The first step in our data reduction was bias subtraction. We monitored the bias level by taking 60 s snaps of a cold dark slide at 30–40 minute intervals. In addition to a steady variation at the 2%–3% level over a 12 hr period, the bias level exhibited two drops, one at the beginning of each night as the instrument, dome, and telescope cooled to a stable temperature, and another after filling the liquid cryogen dewars in the middle of each night. The value of bias level to subtract from each frame was chosen by linear interpolation of the measured bias levels closest in time to the actual observation. The second stage in bias subtraction is the removal of structure. To do this, all the bias frames were averaged for the run to produce a “superdark” frame. This superdark was then subtracted from all bias frames as a test of the stability of bias structure with time. No change was found over 3 days at the 0.05% level as long as the gate voltage was unchanged (our value was -2.71). With no change in bias structure with time, we elected to subtract the bias level using the superdark frame adjusted for the zeropoint bias from interpolation as stated above.

Next, we flat-fielded the data. Since most frames contained mostly sky background counts with a few stars (5–15), we median-filtered the 16 frames of each grid together and used the result to flat-field that grid.

The next step was sky subtraction. By far, our greatest photometric errors result from variations in the sky background level, which corresponded to 13.5–14.0 mag arcsec $^{-2}$ at K and to 15.0–16.5 mag arcsec $^{-2}$ at J . For frames judged to be free of nebular emission, we subtracted the median sky value from each. For frames with nebular emission, we used the sky values obtained from emission-free frames taken closest in time to the nebular frames.

Software aperture photometry was then performed on each individual frame, allowing an internal photometry consistency

check for stars which appeared in two or more frames. Circular software apertures were set to radii of 2–10 pixels, in 1 pixel steps. The final photometric values quoted in this paper are for circular software apertures with 3 pixel radii (corresponding to 8" diameters). The worst internal inconsistencies we found were for faint stars and amounted to differences of 0.5 mag. This was certainly due to intermittent high cirrus during the last two nights. During stable sky conditions, photometry of the same star appearing in different frames was found to be reproducible at the few hundredths of a magnitude level.

Positions for the cluster members were derived from the K mosaic image directly. The six VLA sources of Becker & White (1988) which were detected were used to solve for the pixel to equatorial coordinate conversion. Barring systematic errors, our absolute astrometry would be good to $\approx 1''$. However, the frames in the mosaic that had no common stars were overlapped by the nominal 15" telescope offsets. This procedure introduces systematic astrometric error from two effects: telescope drift and absolute telescope pointing error. Telescope drift caused systematic offsets between frames of one 4×4 grid, whereas absolute pointing errors caused systematic offsets between grids. Typical values for the magnitude of these systematic offsets can be estimated from those few stars which ought to overlap in two adjacent frames, but actually do not because the frames containing them were mosaiced together from their nominal positions. Readers should be warned that systematic offset errors of as much as $10''$ – $15''$ may be present in the coordinates tabulated in Tables 2–5. Accurate source coordinates not suffering from such systematic error await the observation of the surveyed field with the newer, large format IR array cameras.

3. RESULTS

Figure 1 (Plate 2) shows the J mosaic of the LkH α 101 region, covering an $8' \times 12'$ area, which corresponds to 1.9×2.8 pc at the source. Figure 2 (Plate 3) shows the corresponding K mosaic. There are 330 sources detected in the J image and 375 in the K image, excluding LkH α 101. Since 96 sources were detected in K , but not in J , there were 51 J sources not detected at K . These J sources have been omitted from further analysis, since they are most likely foreground, main-sequence stars. We estimate our completeness limits to be 16.5 mag at J and 14.5 mag at K , although sources as faint as $K = 16.0$ and $J = 17.5$ were detected in a few frames.

Figure 3 shows a contour plot of the number density of sources per square arcminute over the survey area. Contour levels are at 6, 8, 10, 12, 14, and 16 stars arcmin $^{-2}$. Peaks in the stellar surface density occur in two frames, each containing 18 stars. These are labeled "Peak 1" and "Peak 2" in Figure 3. As a reference point, the position of LkH α 101 is indicated by the filled square. There is a clear concentration of source counts in the environs of LkH α 101, where there are roughly 4 times as many sources per unit area as at the edges of the mosaic. This spatially coherent enhancement in the K source counts is indicative of a physically associated grouping of stars, and not just to detection of random, highly obscured, background objects.

Ideally, we would like to have compared the star distribution with the gas column density distribution over the entire region to get a clear understanding of the effects of variable extinction on the star counts in the observed area. Although previous CO $J = 1 \rightarrow 0$ observations of the LkH α 101 region exist, they are of too coarse a resolution (Christie, McCutcheon, & Chan 1982) or of only one isotope over a

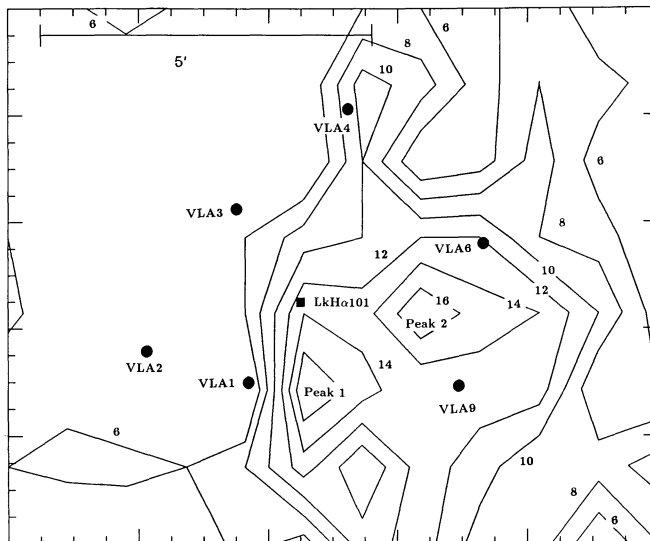


FIG. 3.—Infrared Source Density in the LkH α 101 Region. Contour plot of the K source counts of the mosaic presented in Fig. 2. Contour levels are placed at 6, 8, 10, 12, 14, and 16 K sources arcmin $^{-2}$. Sites marked "Peak 1" and "Peak 2" each correspond to maxima of 18 K sources arcmin $^{-2}$. We have marked the K sources which have known, compact, radio-continuum emission following the nomenclature of Becker & White (1988).

significant fraction of our survey area (Knapp et al. 1976; Redman et al. 1986). The only extant column density map at the required angular resolution of $\leq 1'$ (derived from both CO and ^{13}CO data) covers just the central $2' \times 2'$ region of our field (Barsony et al. 1990). A juxtaposition of this column density map (Fig. 12 of Barsony et al. 1990) on our Figure 3 reveals a rise in column density to the east of LkH α 101, just where the star counts drop off sharply in the region between VLA1 and VLA3. Future mapping of this area at $\leq 1'$ resolution in CO and ^{13}CO would give us great insight into the relation of the gas to the embedded stellar population in this source.

We have also plotted in Figure 3 the locations of those radio continuum sources which we detected in the near-infrared. We have found near-infrared counterparts to six of the nine known weak, compact radio sources recently discovered in the region. Only four of the nine VLA sources have been identified to date: a B2 star (VLA4), two T Tauri stars (VLA3 and VLA6), and an extragalactic double (Becker & White 1988). We detected all of these identified sources, except the extragalactic double (= VLA5). The Galactic VLA sources associated with LkH α 101 that we detected are quite bright at K (see Table 1).

In order to distinguish between unassociated sources and "cluster" members in a statistical sense, we plotted histograms of the apparent J and K brightnesses of all the sources and of all the sources from the frames which contained fewer than 5 sources arcmin $^{-2}$. These latter defined the shape of the J and K distributions labeled "background" in Figures 4 and 5, respectively. To "normalize" the background source histograms, we just multiplied the distributions obtained from sources found in the sparsely populated frames (< 5 sources arcmin $^{-2}$) by the ratio of total area/sparsely populated area. For each filter, the cluster member distribution was derived by subtracting the background star histogram from the histogram containing all the sources. Integration under the histograms marked "cluster members" yields 76 sources at J and 95 sources at K . It is on this basis that we claim there are ≈ 100 cluster members in the survey area.

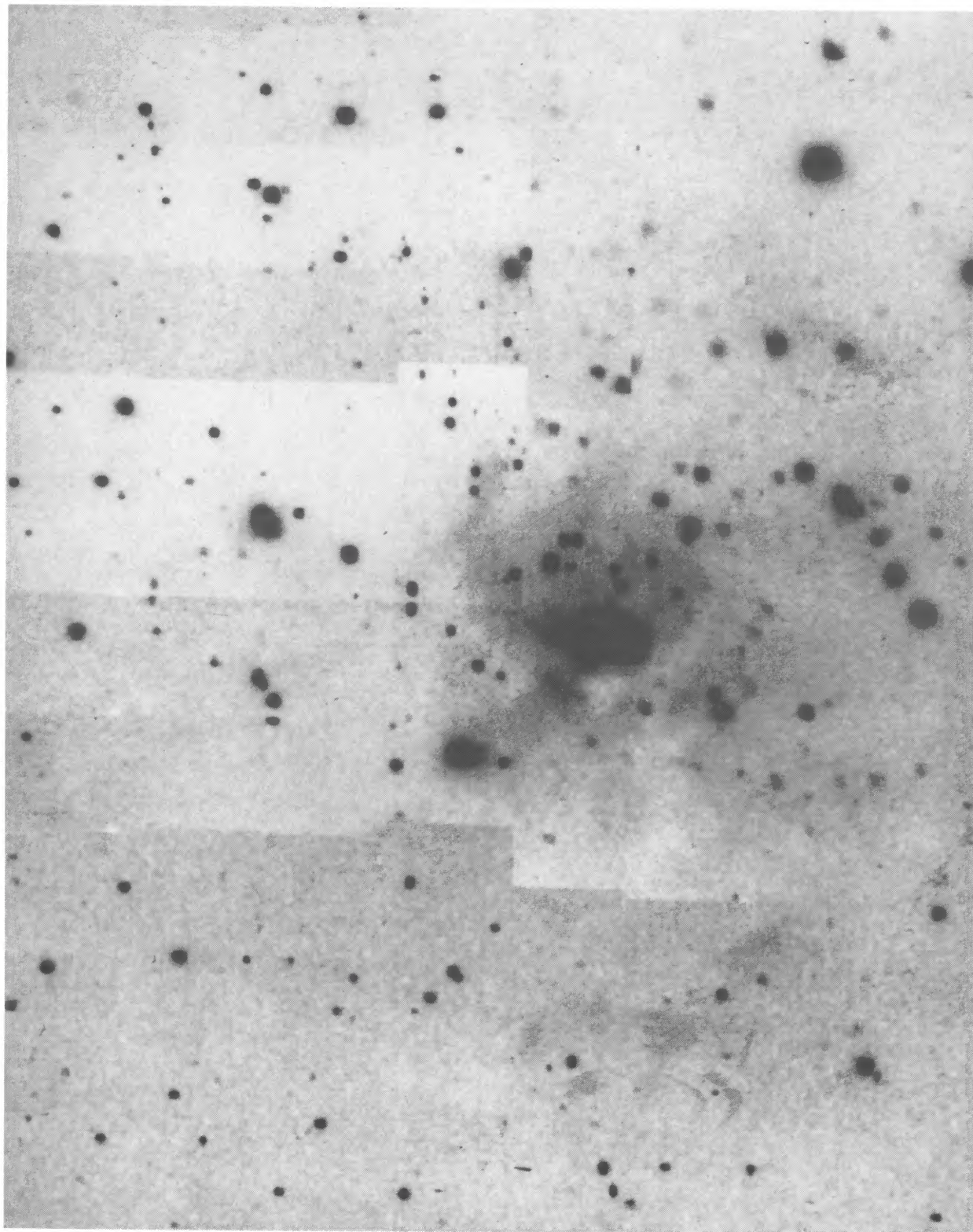


FIG. 1.—The J ($\lambda_0 = 1.2 \mu\text{m}$, $\Delta\lambda = 0.27 \mu\text{m}$) mosaic of the LkHx 101 region consists of 96 frames and covers an area $8' \times 12'$. The bright, nebulous source just south of center is LkHx 101. Excluding LkHx 101 itself, 330 sources were detected in this field.

BARSONY, SCHOMBERT, & KIS-HALAS (see 379, 223)

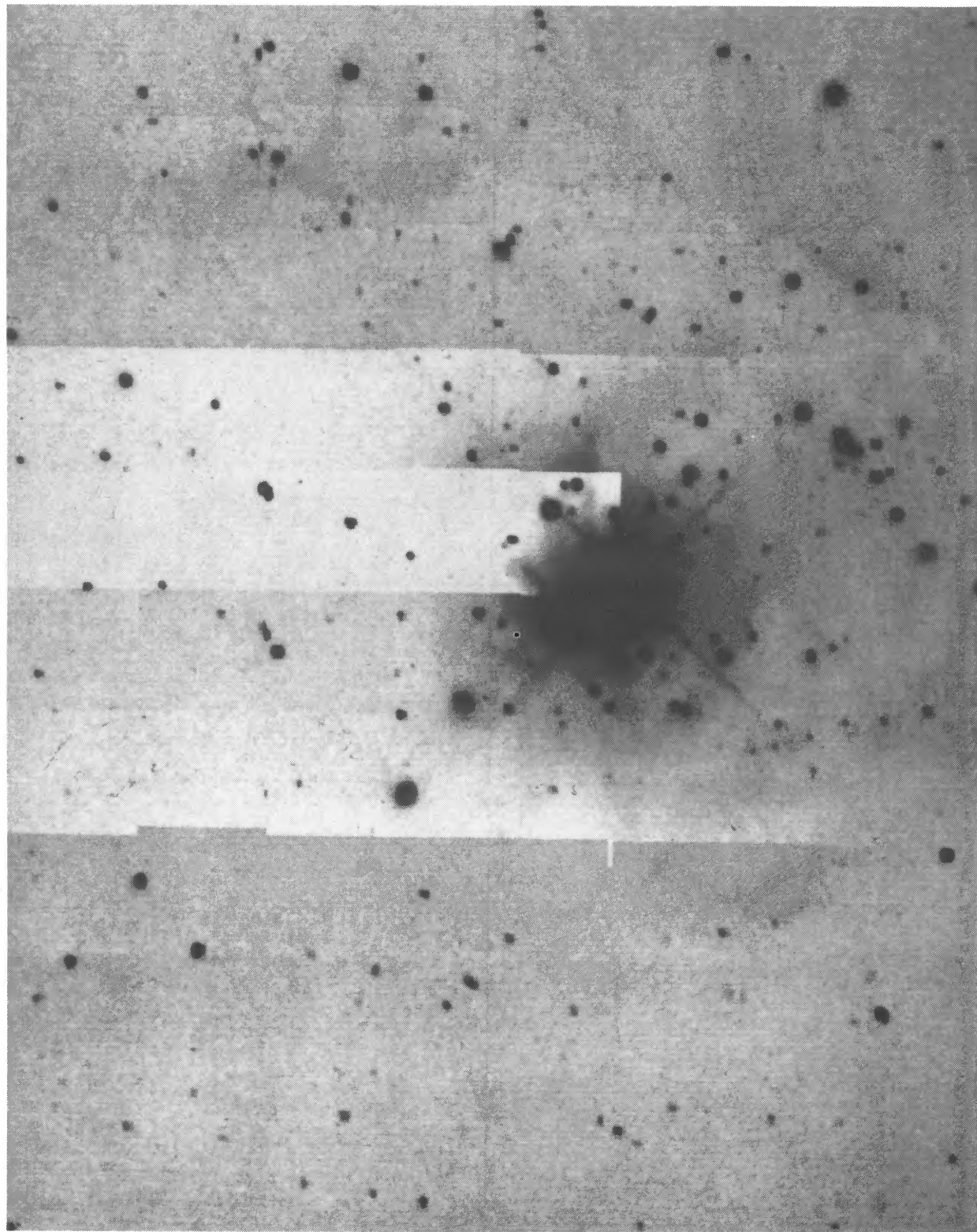


FIG. 2.—The K ($\lambda_0 = 2.2 \mu\text{m}$, $\Delta\lambda = 0.38 \mu\text{m}$) mosaic of the LkHr 101 region corresponding to the J mosaic of Fig. 1. Excluding LkHr 101, 375 sources were detected in this field.

BARSONY, SCHOMBERT, & KIS-HALAS (see 379, 223)

TABLE 1
VLA SOURCES IN THE LkH α 101 FIELD

Source	J	K	$J-K$	Comments ^a
VLA1.....	12.75	10.88	1.87	...
VLA2.....	15.25	12.66	2.59	...
VLA3.....	9.84	8.54	1.30	Spectroscopically determined TTS
VLA4.....	9.68	8.89	0.79	Spectroscopically determined B2 star
VLA5.....	Extragalactic double
VLA6.....	10.64	9.34	1.30	Spectroscopically determined TTS
VLA7.....
VLA8.....
VLA9.....	12.40	9.97	2.43	Heavily reddened star; not visible on blue POSS plate, but visible on red POSS plate

^a Becker & White 1988.

When comparing the histograms of the background sources and the cluster member sources of Figures 4 and 5, note that the peaks of the cluster member distributions are always at brighter magnitudes than the peaks of the background source distributions. The J background star distribution peaks at $J \approx 14.5$ with a long tail toward fainter magnitudes, whereas the cluster member J distribution peaks at $J \approx 13.5$. Similarly the K background distribution peaks at $K \approx 13.5$, while the K cluster member distribution peaks close to $K \approx 11.5$, with a long tail. The background sources peak around a $J-K$ value of 1.0, whereas the cluster member sources peak near a $J-K$

value of 2.0. Since one would expect young, pre-main-sequence stars to be intrinsically brighter and redder than corresponding stars on the main sequence, these results lend support to the validity of our statistical method of separating cluster members from galactic background sources.

A useful way of determining the probable evolutionary status of the LkH α 101 cluster stars is with the aid of color-magnitude diagrams. We have therefore plotted all the stars in the field in a J versus $J-K$ diagram, along with stars for which we have only upper limits at J , indicated by the solid, downward-pointing, triangles (see Fig. 6).

In this same figure we have plotted the position of an unreddened main sequence at 800 pc along with a main sequence at the same distance seen through 10 mag of visual extinction. Note that the average visual extinction over our survey area lies in the range of $2 < A_V < 4$ as determined from star counts of the Palomar Survey blue and red plates (Christie et al. 1982).

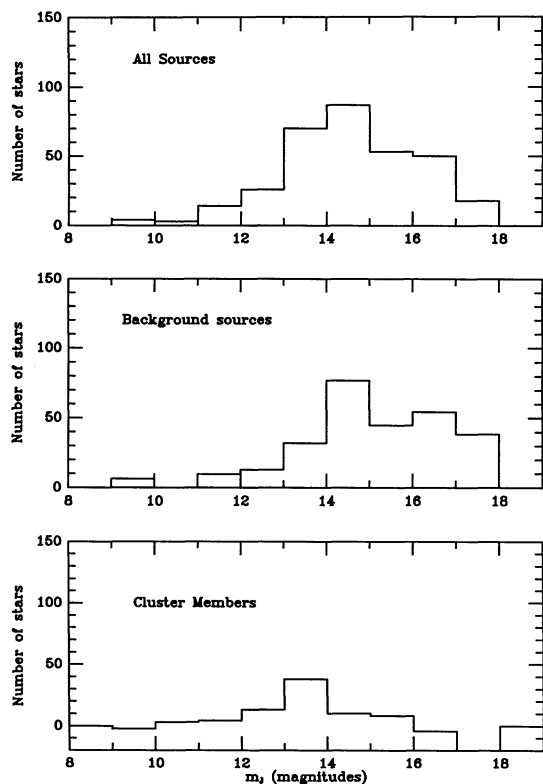


FIG. 4.—Histograms of the distribution of J magnitudes of the sources shown in Fig. 1 for LkH α 101. Top panel includes all 330 sources observed at J . Second panel includes all sources from sparsely populated frames (≤ 5 sources arcmin $^{-2}$), scaled by the ratio of the total area/sparsely populated area, and is taken as statistically representative of the background. Cluster member distribution of the bottom panel is derived by subtracting the background source distribution from the distribution of all sources in the field. Note that the peak of the cluster member distribution is 1 mag brighter than the peak of the background distribution.

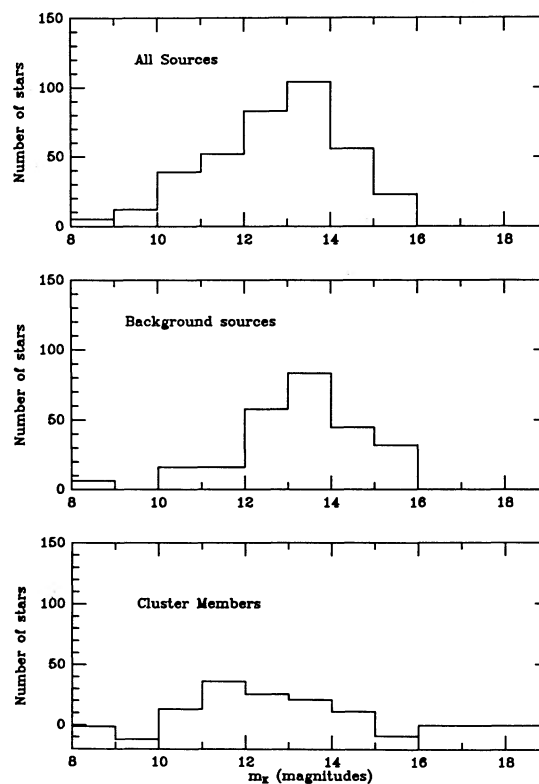


FIG. 5.—Same as for Fig. 4, except at K (sources shown in Fig. 2)

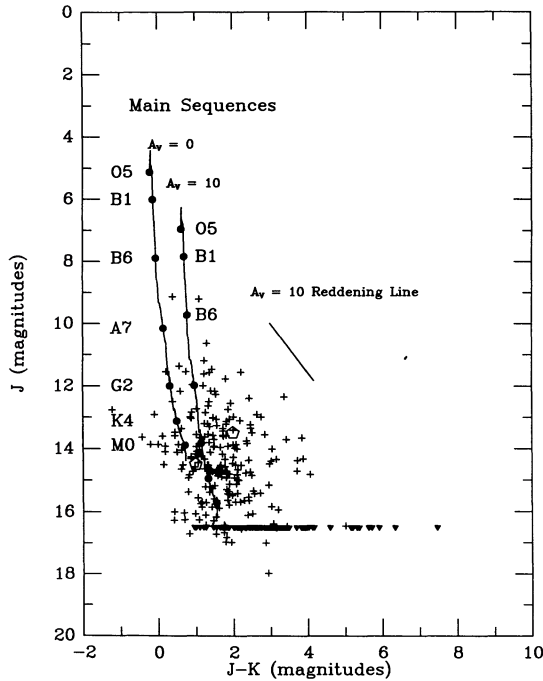


FIG. 6.—Stellar Content of the LkH α 101 Field. The J vs. $J-K$ color-magnitude diagram of the LkH α 101 cluster. The two curves indicate where main-sequence stars would be found if they were located at the same distance as LkH α 101, with either no extinction, or with 10 mag of visual extinction, respectively. The locations of some spectral types are indicated on each main-sequence locus by the filled circles. Corresponding spectral types along the curves may be found with the aid of the $A_V = 10$ reddening line illustrated in the figure. The two open pentagons represent the peak of the background source distribution (at $J = 14.5$, $J-K = 1.0$) and the peak of the cluster member distribution (at $J = 13.5$, $J-K = 2$). The downward-pointing solid triangles represent sources which were detected at K , but not at J .

The A_V to LkH α 101 itself is probably close to 9.4 mag whereas the *total* visual extinction through the cloud along this line of sight (in a $45''$ beam) is estimated to be 43 mag (Barsony et al. 1990).

The position of a star at the peak of the statistically determined background distribution is indicated in Figure 6 by an open pentagon at $J = 14.5$, $J-K = 1.0$ (which is rather hard to see due to source crowding in this region of the diagram). The open pentagon plotted at $J = 13.5$, $J-K = 2.0$ indicates the peak of the cluster member distribution. The relative position of these two points is highly suggestive: the position of the representative background source is consistent with being a distant, slightly reddened, main-sequence star, whereas the position of the typical cluster member is consistent with being a deeply embedded pre-main-sequence star! (Recall that translation of either the $A_V = 0$ or 10 main-sequence curves downward by 2 mag in Fig. 6 is equivalent to moving the respective populations a factor of 2.5 further away than the distance to LkH α 101.)

To further explore the nature of the near-infrared sources in the LkH α 101 field, we have plotted a K versus $J-K$ color-magnitude diagram in Figure 7. Sources detected at K , but with only upper limits at J ($J > 16.5$), are indicated by the solid triangles pointing sideways. The vertical curves marked $A_V = 0$, 10, and 50, respectively, correspond to main sequences suffering these amounts of extinction at 800 pc. The circled stars descending vertically downward from $K \approx 14$ near $J-K = 2$ represent 10^6 year-old brown dwarfs ($0.01-0.1 M_\odot$) suffering

$A_V = 10$ at 800 pc (Nelson, Rappaport, & Joss 1986). For comparison, we have also plotted on the same diagram the location of several famous Class I sources in ρ Oph, translated to the distance of LkH α 101 (Wilking & Lada 1983; Wilking et al. 1989).

In Figure 8 we have divided the K versus $J-K$ diagram into four distinct regions: (1) $J-K > 4$, (2) $3 < J-K < 4$, (3) $2 < J-K < 3$ and $K > 13.4$, and (4) $2 < J-K < 3$ and $K < 13.4$. Hayashi tracks (adapted from Straw, Hyland, & McGregor 1989) translated to an 800 pc distance and obscured by $A_V = 10$ mag are indicated for different stellar masses. The tracks start at 10^5 yr and end in filled circles which mark ages of 10^6 yr.

Sources with $J-K > 4$ are certain to be Class I sources. Since they also happen to be bright ($K < 12$), other explanations for the colors and magnitudes of these sources, such as that they are all red giants suffering more than 50 mag of visual extinction, are untenable.

Similarly, sources with $3 < J-K < 4$ (all but two being brighter than $K \approx 14$) would all have to be of spectral type earlier than A7 (or B6) seen through $A_V = 40$ at 800 pc (or 2 kpc). We conclude that these objects are also most probably Class I sources.

The area designated “ $< 10^6$ yr PMS stars” in Figure 8 corresponds to the location of the relatively bright ($K < 13.4$) sources with $2 < J-K < 3$. The fact that this area lies to the

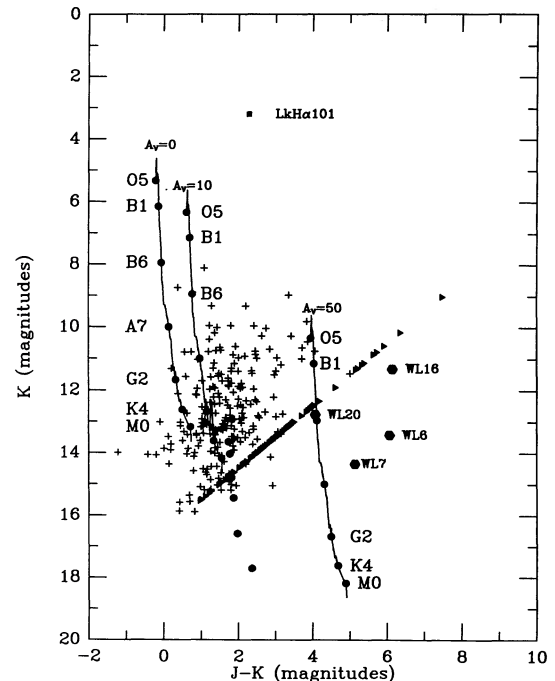


FIG. 7.—Stellar Content of the LkH α 101 Field. The K vs. $J-K$ color-magnitude diagram of the LkH α 101 cluster. Three main sequences at the distance of LkH α 101 are represented for three different values of the extinction: $A_V = 0$, 10, and 50, since the visual extinction to LkH α 101 itself is thought to be 10 mag, while the extinction through the entire cloud along the line of sight to LkH α 101 is 43 mag (Barsony et al. 1990). Encircled stars near $J-K = 2$ represent 10^6 year-old brown dwarfs (as calculated by Nelson et al. 1986) suffering 10 mag of visual extinction at 800 pc.

They correspond to masses of 0.10, 0.08, 0.06, 0.04, 0.02, and 0.01 M_\odot in descending order of K magnitude. Sideways-pointing, filled triangles represent the sources detected at K , but not at J . Filled hexagons represent typical Class I sources (taken from Wilking & Lada 1983), as they would appear at 800 pc. LkH α 101, by far the brightest member of the cluster, is represented by the filled square.

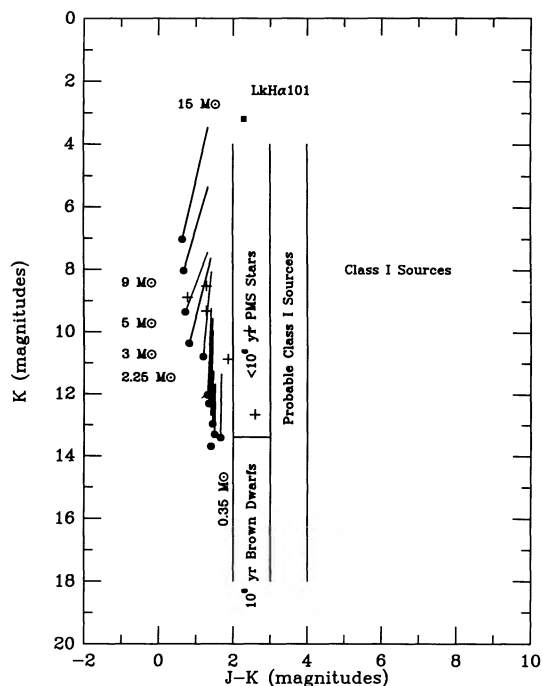


FIG. 8.—Hayashi tracks at 800 pc through $A_V = 10$ (adapted from Straw et al. 1989) as they would appear through 10 mag of visual extinction at the distance of LkH α 101 in the K vs. $J-K$ color-magnitude diagram. Top of the tracks correspond to an “age” of 10^5 yr. The filled circles represent the stage reached at 10^6 yr. Tracks correspond to masses of 15, 9, 5, 3, 2.25, 1.5, 1.25, 1.0, 0.8, 0.5, and 0.35 M_\odot , in descending order from brightest to faintest. Other regions of the diagram, defined for classification purposes in the text, are also indicated. Crosses mark the locations of previously detected radio continuum sources, as listed in Table 1.

right of the Hayashi tracks for embedded. PMS stars is convincing proof of the extreme youth of objects occupying this region of the K versus $J-K$ color-magnitude diagram.

In fact, we are being extremely conservative in our definition of the region occupied by PMS stars. To illustrate this point, refer again to Figure 8. The six crosses indicated in Figure 8 illustrate the location of the VLA radio continuum sources with detections at both J and K . The two known T Tauri stars of this group each have $J-K$ values of only 1.3 (see Table 1). It is therefore likely that *most* of the bright ($K < 12$), red ($J-K > 1$) sources in Figure 7 are pre-main-sequence stars, since they occupy the same area of the K versus $J-K$ color-magnitude diagram as the Herbig Ae/Be stars. For comparison, a filled square marks the location of LkH α 101, a known pre-main-sequence (or barely ZAMS) B0 star. Other sources which would occupy this region of the K versus $J-K$ diagram are either background K and M giants, or background, highly obscured ($10 < A_V < 70$) O stars. Since we would expect to see at best one background subgiant or a handful of background O and B stars in our rather small (in Galactic terms) survey area, probably most of these sources are part of the embedded cluster. The following analysis of the *IRAS* results for this region leads to a similar conclusion. Although LkH α 101 is by far the most luminous source in this cloud, it accounts for only 25% of the total *IRAS* luminosity in the region (Barsony et al. 1990). Thus, it is reasonable to expect an embedded population of Herbig Ae/Be stars to account for the rest of the $4.0 \times 10^4 L_\odot$ of the much larger ($33' \times 40'$) *IRAS* emission. Also, note that in the densest regions of Figure 3, there are on the order of 16–18 bright K sources in one *IRAS* 100 μm beam!

Finally, we define the region demarcated by $2 < J-K < 3$ and $K > 13.4$ in Figure 8 as “ 10^6 year-old brown dwarf candidates.” This definition comes from taking brown dwarf evolutionary models (Nelson et al. 1986), assuming they radiate as blackbodies of the given luminosities and effective temperatures, and calculating their expected J and K magnitudes at 800 pc and seen through $A_V = 10$. The results for masses of 0.1, 0.08, 0.06, 0.04, 0.02, and 0.01 M_\odot are represented by the circled stars of Figure 7. The only other sources which would occupy this region of the K versus $J-K$ diagram are background, low-mass, main-sequence stars which would have to be both distant (to be so faint) and heavily extinguished (to be so red). To have $2 < J-K < 3$, a low-mass, main-sequence star would have to have $A_V > 10$. Given that the *average* extinction, derived from star counts, is $2 < A_V < 5$ over our observed field, it is highly unlikely that *all* of the sources occupying this region of the K versus $J-K$ diagram are background stars. The spatial segregation of these sources (58% of them are concentrated in one-sixteenth of the entire survey area) also hints that they are physically associated with each other and with the LkH α 101 cluster.

From Figure 7, we can estimate to what depth in the molecular cloud we could detect different types of sources. With no extinction, any star down to spectral type M8 and $0.08 L_\odot$ out to 2 kpc would have been detected. At $A_V = 10$, we could detect stars to spectral type M8 and $L = 0.08 L_\odot$ to 1.3 kpc. Assuming the greatest extinction through the cloud to be $A_V = 50$, we could detect any main-sequence star down to spectral type A7 and $L = 100 L_\odot$ through the entire cloud (at 800 pc). From the foregoing, it is clear that we have completely sampled the stellar population to $A_V = 20$ in the LkH α 101 cloud core, and that we have completely sampled the entire cloud volume to main-sequence stars of spectral type A7 or earlier. Limits on the detectability of Class I sources are best estimated by noting the positions of the known Class I sources in Figure 7 (which take into account the 800 pc distance to LkH α 101). The luminosities of WL16, WL1, and WL19 are 14, 1.6, and $1.0 L_\odot$, respectively. From this, we estimate our survey to be sensitive (although not necessarily complete) to Class I sources down to $\approx 1.0 L_\odot$.

In Tables 2–5 we present the positions, K magnitudes, and values (or lower limits) of the $J-K$ colors for the cluster members we have classified based upon their location in the K

TABLE 2
CLASS I SOURCES ($J-K \geq 4$)

K	$J-K^a$	R.A. (1950)	Decl. (1950)
12.33.....	>4.17	04 ^h 27 ^m 14 ^s .7	35°08'04"
10.59.....	>5.91	04 26 58.4	35 07 36
10.86.....	>5.64	04 26 55.1	35 08 04
12.37.....	>4.13	04 26 55.0	35 08 18
11.18.....	>5.32	04 27 06.7	35 07 36
11.44.....	>5.06	04 27 00.4	35 10 43
10.87.....	>5.63	04 26 58.8	35 09 35
10.16.....	>6.34	04 26 58.3	35 09 42
12.47.....	>4.03	04 26 53.5	35 08 33
11.29.....	>5.21	04 27 01.0	35 09 44
10.78.....	>5.72	04 27 00.5	35 10 00
12.51.....	>3.99	04 26 58.4	35 11 45
10.76.....	4.07	04 26 32.4	35 08 08
11.46.....	5.01	04 26 33.6	35 09 26
11.9.....	>4.60	04 25 53.0	35 10 35
11.12.....	>5.38	04 26 52.0	35 09 41

^a Upper limits are based on a nondetection at $J \geq 16.5$.

versus $J-K$ color-magnitude diagram. Note that systematic errors are present in the astrometry due to the effects of telescope drift and absolute telescope pointing error on the mosaicing procedure. The magnitude of such systematic error was measured in the case of a few stars which fell on the "seam" between frames in those instances where the part of the star falling on one frame was shifted relative to the part of it appearing on the adjacent frame. The magnitude of such measured shifts varied from a few tenths of a pixel to 5.75 pixels, corresponding to a maximum systematic offset of $\approx 7''$. If no systematic error were present, these few stars would have had identical pixel values at their centers.

4. DISCUSSION

We may draw several interesting conclusions regarding the star formation process from our observations.

The first has to do with the spatial segregation of the embedded population. To illustrate any trends of spatial segregation by age or mass effectively, we have plotted the spatial distribution of each type of source separately. The accreting protostars (sources with $J-K > 4$) are plotted in Figure 9, probable accreting protostars (sources with $3 < J-K < 4$) are plotted in Figure 10, brown dwarf candidates (sources with $K > 13.4$, $2 < J-K < 3$) are plotted in Figure 11, and very young ($< 10^6$ yr) pre-main-sequence stars ($K < 13.4$, $2 < J-K < 3$) are plotted in Figure 12. For reference, in each of Figures 9–12, LkH α 101 is represented by a five-pointed star.

It turns out that 90% (14/16) of the accreting protostars (those with $J-K > 4$) are within 0.7 pc ($\approx 3'$) of LkH α 101 (see Fig. 9). This is our best evidence for age segregation in this cluster. The youngest cluster members seem to be the most centrally concentrated. If this is indeed the case, then we can infer from its location in the cloud that LkH α 101, the most massive star of this cluster, formed relatively late. From its position in the $\log T_{\text{eff}}-\log L$ plane, LkH α 101 was found to be $\approx 10^5$ yr old (Barsony 1989). In the ongoing controversy over whether the most massive stars in a cluster form first or last, our results strongly supported the latter view.

One might argue that the dramatic spatial segregation of the sources with $J-K > 4$ could be due to nothing more than their location in the densest part of the molecular cloud core, and that their extremely red colors are not intrinsic (and there-

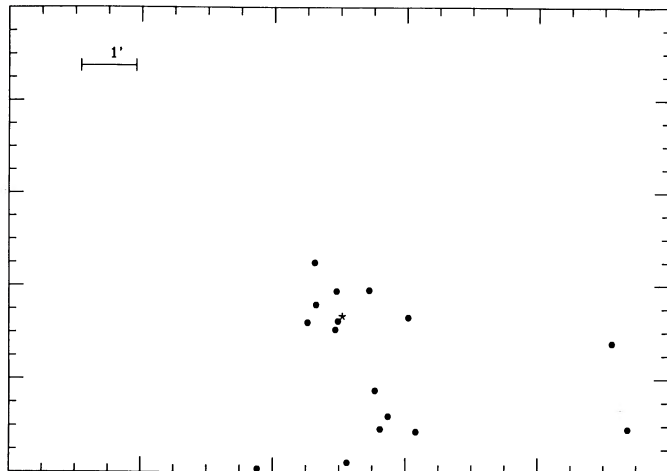


FIG. 9.—Spatial distribution of the 16 accreting protostars (Class I sources) in the LkH α 101 cluster. These are sources with $J-K > 4$. LkH α 101 is represented by the five-pointed star.

TABLE 3
PROBABLE CLASS I SOURCES ($3 \leq J-K \leq 4$)

K	$J-K^a$	R.A. (1950)	Decl. (1950)
12.83.....	3.02	04 ^h 26 ^m 34 ^s .6	35°10'41"
13.32.....	3.07	04 26 47.6	35 10 50
12.75.....	3.20	05 26 47.5	35 08 32
8.98.....	3.37	04 26 54.3	35 10 30
10.65.....	3.73	04 27 02.5	35 09 35
11.00.....	3.72	04 27 02.4	35 09 39
11.19.....	3.16	04 27 00.3	35 09 39
10.97.....	3.05	04 26 59.8	35 09 32
9.81.....	3.85	04 27 00.2	35 09 50
11.39.....	3.02	04 26 57.4	35 13 50
13.39.....	3.15	04 26 35.0	35 13 38
13.04.....	3.44	04 27 26.6	35 12 35
10.28.....	3.43	04 27 09.2	35 14 12
13.05.....	>3.45	04 26 30.9	35 08 37
13.42.....	>3.08	04 26 33.7	35 09 17
12.58.....	>3.92	04 26 49.3	35 11 20
13.32.....	>3.18	04 26 44.1	35 09 32
13.0.....	>3.5	04 26 46.7	35 08 11
12.8.....	>3.7	04 26 44.2	35 08 33
13.17.....	>3.33	04 26 45.3	35 07 44
12.56.....	>3.94	04 26 46.8	35 07 59
13.44.....	>3.06	04 26 44.3	35 08 06
13.00.....	>3.5	n.a.	n.a.
13.47.....	>3.03	n.a.	n.a.
13.38.....	>3.12	04 26 36.5	35 09 05
13.27.....	>3.23	04 26 51.0	35 11 03
12.63.....	>3.87	04 26 53.2	35 08 20
13.43.....	>3.07	04 26 54.9	35 07 34
13.27.....	>3.23	04 26 53.0	35 07 50
13.14.....	>3.36	04 26 55.0	35 08 18
12.52.....	>3.98	04 27 04.2	35 08 59
12.53.....	>3.97	04 27 04.3	35 09 09
13.1.....	>3.40	04 27 04.0	35 09 22
12.62.....	>3.88	04 27 04.1	35 09 22
13.19.....	>3.31	04 26 55.8	35 11 46
13.17.....	>3.33	04 27 06.8	35 11 45
13.49.....	>3.01	04 27 01.8	35 13 49
13.22.....	>3.28	04 26 39.0	35 14 26
12.67.....	>3.83	04 27 21.7	35 12 25

^a Upper limits are based on a nondetection to $J \geq 16.5$.

fore an indicator of youth), but are instead a result of extreme reddening.

However, we must take into account that these sources are also very *bright* (all have $K < 12$). In fact, our "accreting

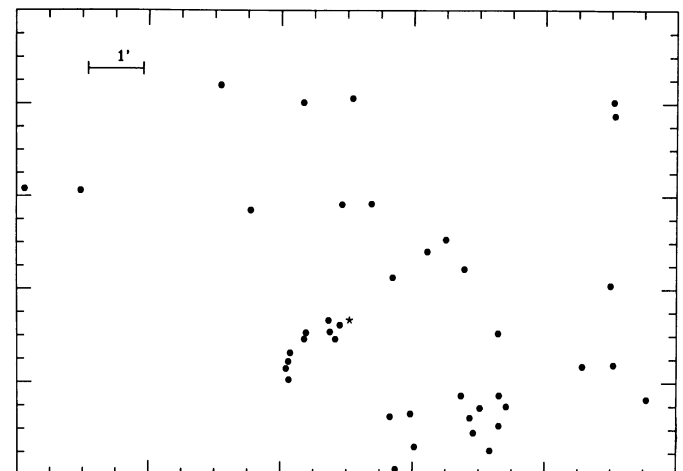


FIG. 10.—Spatial distribution of the probable accreting protostars (Class I sources; those sources with $3 < J-K < 4$) in the LkH α 101 cluster. Location of LkH α 101 is indicated by the five-pointed star.

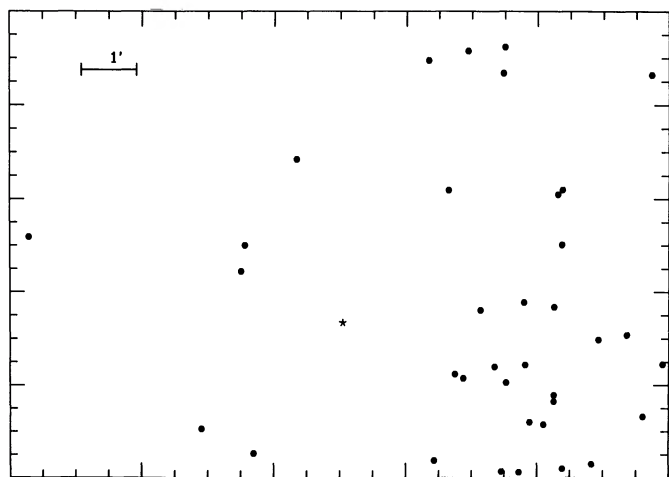


FIG. 11.—Spatial distribution of the brown dwarf candidates in the LkH α 101 cluster. These are sources with $K > 13.4$ and $2 < J - K < 3$. We have plotted only those 36 sources with no J counterparts. Location of LkH α 101 is indicated by the five-pointed star.

TABLE 4

YOUNG ($\leq 10^6$ yr) PRE-MAIN-SEQUENCE STARS
($2 \leq J - K \leq 3$ AND $K < 13.4$)

K	$J - K$	R.A. (1950)	Decl. (1950)
12.69	2.73	04 ^b 26 ^m 35 ^s .9	35°10'39"
12.87	2.57	04 26 38.9	35 10 45
11.9	2.12	04 26 48.7	35 10 29
12.9	2.04	04 26 48.4	35 10 35
12.86	2.15	04 26 46.9	35 10 55
12.36	2.50	04 26 47.2	35 09 25
10.99	2.51	04 26 45.9	35 08 16
9.97	2.43	04 26 45.5	35 08 44
9.34	2.22	04 26 43.3	35 07 24
12.46	2.07	04 26 40.4	35 07 47
11.51	2.98	04 26 38.0	35 08 28
12.3	2.46	04 26 36.2	35 09 16
10.04	2.76	04 26 53.4	35 10 18
10.92	2.19	04 26 53.4	35 10 24
10.97	2.02	04 26 55.5	35 10 49
11.38	2.37	04 26 55.4	35 09 21
10.7	2.86	04 26 56.5	35 09 30
10.77	2.47	04 26 54.3	35 09 45
10.28	2.64	04 26 54.5	35 10 02
12.21	2.96	04 26 55.6	35 08 34
11.96	2.42	04 26 56.2	35 08 57
11.87	2.01	04 26 57.4	35 09 02
11.78	2.09	04 26 59.2	35 09 08
11.93	2.06	04 27 00.4	35 08 33
10.88	1.87	04 27 00.7	35 08 42
11.46	2.38	04 26 59.6	35 09 05
10.87	2.48	04 26 59.8	35 09 20
12.72	2.11	04 26 48.2 ^a	35 11 19 ^a
13.04	2.09	04 26 54.7	35 15 03
12.44	2.34	04 26 56.0	35 15 30
12.54	2.13	04 26 49.7	35 14 50
13.24	2.42	04 26 45.7	35 12 04
12.87	2.13	04 26 42.1	35 12 10
13.31	2.12	04 26 43.2	35 12 27
12.81	2.54	04 26 30.2	35 13 38
13.35	2.30	04 26 33.4	35 14 12
12.27	2.01	04 27 11.7	35 09 29
13.14	2.41	04 27 11.8	35 09 53
11.4	2.01	04 27 13.2	35 11 24
12.32	2.22	04 27 23.3	35 15 46

^a But 04^b26^m43^s.3 and 35°11'45" from another frame.

TABLE 5

YOUNG ($< 10^6$ yr) BROWN DWARF CANDIDATES
($2 \leq J - K < 3$ AND $K > 13.4$)

K	$J - K^a$	R.A. (1950)	Decl. (1950)
13.64	2.06	04 ^b 26 ^m 55 ^s .4	35°14'14"
13.52	2.99	04 26 48.7	35 15 12
14.36	2.21	04 26 34.4	35 12 03
13.73	2.39	04 26 44.4	35 13 19
13.51	2.19	04 26 44.5	35 14 19
14.14	2.87	04 27 14	35 12 21
13.57	2.51	04 27 24.9	35 12 25
15.05	2.93	04 27 15.3	35 14 47
14.18	> 2.32	04 26 34.2	35 08 31
14.46	> 2.04	04 26 29.8	35 09 17
14.40	> 2.10	04 26 34.1	35 09 31
14.29	> 2.21	04 26 31.8	35 09 38
14.27	> 2.23	04 26 38.4	35 10 00
14.37	> 2.13	04 26 37.9	35 11 18
13.88	> 2.62	04 26 44.8	35 09 52
13.59	> 2.91	04 26 46.5	35 08 47
13.74	> 2.76	04 26 47.4	35 08 51
13.54	> 2.96	04 26 43.8	35 08 58
14.0	> 2.5	04 26 42.3	35 07 24
13.88	> 2.62	04 26 43.9	35 07 27
14.14	> 2.36	04 26 40.7	35 08 10
14.28	> 2.22	04 26 39.6	35 08 07
13.64	> 2.86	04 26 38.1	35 07 32
13.68	> 2.82	04 26 35.6	35 07 37
13.93	> 2.57	04 26 38	35 08 28
13.56	> 2.94	04 26 38.6	35 08 35
14.05	> 2.45	04 26 41.1	35 09 50
14.48	> 2.02	04 26 40.9	35 10 02
13.6	> 2.90	04 26 42.8	35 08 44
13.91	> 2.59	04 26 41	35 09 01
13.93	> 2.57	04 26 49.9	35 10 57
13.6	> 2.9	04 26 50.8	35 07 39
13.98	> 2.52	04 27 07.4	35 07 59
14.04	> 2.46	04 27 07.2	35 11 04
14.38	> 2.12	04 27 06.9	35 11 20
13.79	> 2.71	04 26 57.1	35 11 57
13.85	> 2.65	04 26 56.8	35 12 01
14.08	> 2.42	04 27 07.1	35 12 06
14.33	> 2.17	04 27 05.7	35 14 50
13.53	> 2.97	04 27 02.5	35 14 55
14.36	> 2.14	04 27 02.2	35 14 19
13.84	> 2.66	04 26 49.3	35 14 21
14.05	> 2.45	04 26 42.8	35 12 35
13.53	> 2.97	04 26 31.6	35 14 49
13.9	> 2.6	04 27 11.5	35 08 20
14.16	> 2.34	04 27 16.8	35 12 17

^a Upper limits are based on a nondetection to $J \geq 16.5$.

protostellar" sources are generally brighter, as a class, than the T Tauri stars (see Fig. 7). This trend of a correlation of K brightness with $J - K$ color has also recently been noted in the context of PMS binaries (Moneti & Zinnecker 1991). The obvious interpretation is that the extra luminosity is from accretion.

Suppose, for the sake of argument, that we were to accept the explanation that our Class I sources are observed to have $J - K > 4$ because they are all very heavily extinguished. Then a cluster source as bright as LkH α 101 would have to suffer 100 mag of visual extinction to have an observed $K \approx 12$. In other words, if we were to accept the explanation that all our Class I sources are red because they suffer 50–100 mag of visual extinction, we would also have to infer that they were intrinsically nearly as bright as LkH α 101 to account for their observed bright K magnitude. If they truly were so bright intrinsically, we would also expect to detect their ionizing radiation with

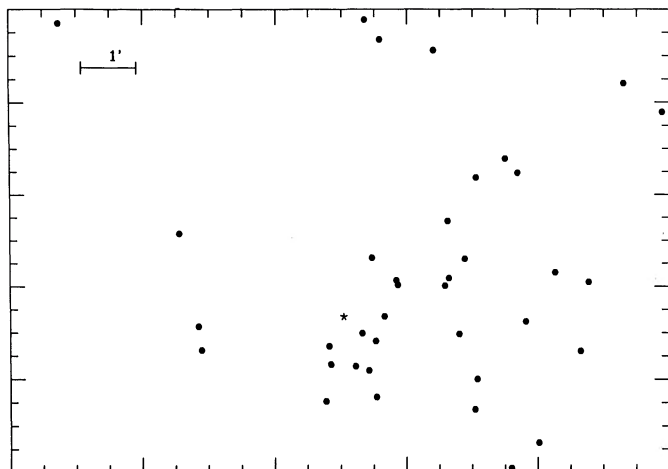


FIG. 12.—Spatial distribution of the very young ($<10^6$ yr) pre-main-sequence stars in the LkH α 101 cluster. These are sources with $K < 13.4$ and $2 < J - K < 3$. Location of LkH α 101 is indicated by the five-pointed star.

VLA measurements. To date, none of these Class I sources have been detected with the VLA.

An observational project which could help distinguish whether or not the observed red colors of our Class I sources are due to foreground or intrinsic reddening would be to obtain a good, high-resolution ($<1'$) column density map of our survey region. A detailed comparison of the column density distribution with the location of the different types of source we have classified would clarify this issue. We have already indicated that a comparison of the existing column density map of the central $2' \times 2'$ region surrounding LkH α 101 (Fig. 12 of Barsony et al. 1990) with our Figure 3 revealed a drop-off in star counts with increasing column density. The Class I sources are actually found near a peak in the K star counts. In sum, preliminary indications are that our Class I sources are, indeed, intrinsically red, and, therefore, young, although further work on this issue is currently in progress.

The 39 “probable Class I sources” (those with $3 < J - K < 4$) of Figure 10 also exhibit spatial segregation in the sense that 79% (31/39) of them lie within 33% of the total survey area, near LkH α 101. Of these 31, 15 are coextensive with the Class I sources.

Of the 40 young ($<10^6$ yr) PMS sources (those with $2 < J - K < 3$ and $K < 13.4$) of Figure 11, 22 (or 55%) are within the same 33% of the total survey area as the “probable Class I sources” of Figure 10. Of these 22, 12 are coextensive with the Class I sources.

There is a significant spatial overlap among the Class I, probable Class I, and very young PMS sources. However, the probable Class I and the very young PMS sources are spatially more widely scattered than the Class I sources alone. There is no obvious difference in how the very young PMS and the probable Class I sources are distributed spatially.

Finally, of the 46 young, embedded, brown dwarf candidates, 21 (46%) are with 17% of the survey area. If we exclude the eight sources in this group which have J counterparts as probable background sources, then 21/38 or 55% of the brown dwarf candidates occupy 17% of the surveyed area. If these sources were randomly distributed, we would have found six instead of 21 sources in this small region. In other words, we have found a 3.5σ peak over the “background” source counts for very faint red sources in this region. This observed high

degree of spatial clustering is a good argument that these sources must be physically associated with the LkH α 101 cluster, and not just chance background sources. In Figure 12, we have plotted only those brown dwarf candidates that have no detectable J counterparts.

There is some marginal evidence for mass segregation in the cluster, in the sense that the least massive stars (the young brown dwarf candidates) are generally further from LkH α 101 than the other types of sources. None of the young ($<10^6$ yr), embedded ($A_V \approx 10$) brown dwarf candidates are spatially coextensive with the Class I sources, whereas 12 of the young PMS sources and 15 of the probable Class I sources are. We must be careful of selection effects, however, since the area near LkH α 101 is contaminated by nebular emission, making the detection of very faint sources difficult. Although the presence of the nebular emission could be responsible for the lack of detection of very faint sources in the immediate environs of LkH α 101, it cannot account for the obvious larger areal spread of the probable Class I and young PMS sources relative to the Class I sources. The observed differences in the spatial extents of the various types of sources could be explained by age and/or mass segregation effects.

We can use our observations of the LkH α 101 cluster to place a stringent upper limit on the cluster age based on kinematic considerations. Cluster stars usually have velocity dispersions of a few km s^{-1} (Blaauw 1964; Lada & Lada 1991). If the velocity vectors of the cluster stars point in random directions, then a star with a 1 km s^{-1} motion in the plane of the sky would leave the field we surveyed in 2×10^6 yr. In other words, the cluster would no longer be recognizable as such after a 2×10^6 yr period. We have, of course, assumed the cluster, as a whole, to be gravitationally unbound.

Another hint as to the extreme youth of the LkH α 101 cluster comes from recent models of the evolution of pre-main-sequence star clusters (Stahler 1991, private communication). In these models, the number of protostars in a cluster reaches a steady state value within a few free-fall times. Thereafter, the fraction of protostars/all stars in the cluster declines in the same ratio as the accretion time/cluster age. If we take the infall rate for a $0.1 M_\odot$ star to be $10^{-6} M_\odot \text{ yr}^{-1}$, then a typical accretion time would be 10^5 yr, and a ratio of 16 protostellar sources/141 cluster members would imply a cluster age of 8.6×10^5 yr.

We can also estimate the time a typical star spends in the protostellar collapse (Class I) phase from the relative numbers of the types of sources we have identified. The Class I and probable Class I sources account for 55 (39%) of the 141 sources we have classified. If we assume a constant star formation rate over the last 10^6 yr, then the average time spent in the protostellar accretion phase is ≈ 0.4 of the average age of the young, PMS stars ($\leq 10^6$ yr), or $< 4 \times 10^5$ yr. This is in good agreement with the average age of $3.9 \pm 1.7 \times 10^5$ yr for a Class I source derived by Wilking et al. (1989), based on relative numbers of Class I and T Tauri sources in ρ Oph.

We derive an upper limit of $(2.7 \times 10^{17} \text{ cm}^3)^3$ for the initial volume of gas which could have collapsed to form stars near the cluster center. This number is derived in the following manner. The highest stellar surface density of $18/(0.23 \times 0.24 \text{ pc})$ is observed near LkH α 101 itself. If we assume these embedded stars to be uniformly distributed throughout the available volume, then the stellar volume density is simply $18/(0.23 \text{ pc})^3$, or one star every $2.7 \times 10^{17} \text{ cm}^3$. If the collapse had proceeded from a larger initial volume, the gas parcel in question would

have come under the gravitational influence of more than one center of collapse.

For comparison, the corresponding maximum initial volume for matter to fall in to form a star in the ρ Oph cloud core is $61/(0.56 \text{ pc})^3$, or one star every $(4.4 \times 10^{17} \text{ cm})^3$ (Barsony et al. 1990). For the Trapezium cluster in Orion, this value is $100/(0.1 \text{ pc})^3$ or one star every $(6.65 \times 10^{16} \text{ cm})^3$ (McCaughrean 1989). Corresponding values in the L1630 cloud are one star every $(6.5 \times 10^{17} \text{ cm})^3$ for the densest part of the NGC 2071 cluster one star every $(6.4 \times 10^{17} \text{ cm})^3$ in the densest part of the NGC 2068 cluster, and one star every $(3.1 \times 10^{17} \text{ cm})^3$ in the densest part of the NGC 2024 cluster (Lada et al. 1991). In its densest parts, the LkH α 101 cluster is as dense as the NGC 2024 cluster.

In Taurus, regions with the highest stellar density are found in cold cores of $\approx (0.2 \text{ pc})^3$ extent which are associated with at most four $2 \mu\text{m}$ sources (Myers 1990, private communication). The corresponding maximum stellar density is 1 star every $(3.9 \times 10^{17} \text{ cm})^3$.

As stated in the Introduction, a natural assumption to explain high-mass star formation is that more massive stars collapsed from larger initial volumes than less massive stars. The available evidence emerging from near-infrared array camera studies of currently forming young clusters, including the present study of the LkH α 101 cluster, actually points to the contrary: the birthplaces of the most massive stars are those with the densest stellar populations, and therefore, those with the smallest allowed initial collapse volumes. An alternate suggestion, which so far is borne out by the observations (Lada, Bally, & Stark 1991), is that the most massive stars form from the *densest*, rather than from the largest, clumps. Clearly, further high-resolution surveys of dense gas tracers in both high- and low-mass star-forming regions are called for to substantiate this claim.

If the original cloud from which these clusters form starts with a large-scale (over several parsecs) centrally peaked density distribution, such that the cloud core outer regions have $n_{\text{H}_2} \approx 10^3 \text{ cm}^{-3}$ while its central regions approach $n_{\text{H}_2} \approx 10^5 \text{ cm}^{-3}$, one might then expect the relatively lower mass stars to be forming further out from the cloud center and the higher mass stars to be more centrally concentrated.

What constraints, if any, do our results place on theoretical considerations of the star formation process? We may derive protostellar collapse rates from the upper limit on the initial collapse volume $(2.7 \times 10^{17} \text{ cm})^3$ we derived above. Assuming initially uniform hydrogen molecular densities of 10^3 , 10^4 , and 10^5 cm^{-3} , this initial collapse volume corresponds to masses of 0.045, 0.45, and $4.5 M_\odot$, respectively. If we further assume that our derived upper limit of $4 \times 10^5 \text{ yr}$ for the protostellar collapse phase is mass-independent, and that the mass infall rate is constant, we deduce corresponding accretion rates of 1.1×10^{-7} , 1.1×10^{-6} , and $1.1 \times 10^{-5} M_\odot \text{ yr}^{-1}$.

The upper limits we have derived for the duration of the protostellar collapse phase and for the volume of gas which can eventually collapse to form a single star are consistent with the values adopted for a typical self-similar collapse calculation for a protostar (Shu 1977). For an external pressure of $P_{\text{ext}}/k = 1.1 \times 10^5 \text{ cm}^{-3} \text{ K}$ and sound speed of $a = 0.2 \text{ km s}^{-1}$, the self-similar collapse solution resulted in an initial infall radius of $1.6 \times 10^{17} \text{ cm}$ (or a volume of $[3.2 \times 10^{17} \text{ cm}]^3$ in our terminology) and a mass of $0.96 M_\odot$ (recall that the density distribution in this instance was assumed to be that of a singular, isothermal sphere). The collapse time for this solution was $2.5 \times 10^5 \text{ yr}$.

Finally, a note on star formation efficiencies. In the central $2' \times 2'$ region of the LkH α 101 cloud core, there are $\approx 112 M_\odot$ of molecular gas (Barsony et al. 1990). In this same area, we observe 20 embedded sources in addition to LkH α 101, which is a 12–15 M_\odot PMS star. Assuming an average stellar mass of $0.5 M_\odot$, the total mass in stars in this central region is $\approx 25 M_\odot$, which translates to a star formation efficiency, $M_*/(M_* + M_{\text{gas}})$, of 18%.

5. CONCLUSIONS

We have discovered a young ($\approx 10^6 \text{ yr}$ old), embedded star cluster surrounding the emission-line Herbig Ae/Be star, LkH α 101, from a deep, near-infrared survey. Of the 375 sources detected at K ($2.2 \mu\text{m}$) in an $8' \times 12'$ field, ≈ 150 sources are cluster members. These sources can further be classified according to their location in a K versus $J-K$ color-magnitude diagram into four types of objects: accreting protostars, probable accreting protostars, less than 10^6 yr old pre-main-sequence stars, and less than 10^6 yr old brown dwarf candidates.

We find evidence for age segregation in this cluster. The spatial distribution of the accreting protostars is highly centrally concentrated near LkH α 101. The older sources, including the T Tauri stars initially discovered via their radio continuum emission, are distributed over a much larger area. We also find some evidence of mass segregation in this cluster. The most massive source, by far, is LkH α 101, which is a 10^5 yr old, 12–15 M_\odot , pre-main-sequence star. The brightest (and, presumably, the most massive sources) are near LkH α 101. The centroid of the young brown dwarf candidate spatial distribution, however, is displaced from LkH α 101 by about 1 pc. This latter result is still inconclusive, in that the bright nebulosity associated with LkH α 101 makes detection of very faint sources near it difficult. However, we can justifiably conclude that the most massive stars in this cluster are forming last.

We have found an upper limit to the initial volume of gas from which a star could eventually form of $(2.7 \times 10^{17} \text{ cm})^3$ in the densest parts of the cluster.

The upper limit to the length of the protostellar collapse phase in this cluster is $4 \times 10^5 \text{ yr}$.

We speculate that a necessary *initial* condition for the formation of a massive versus the formation of an ordinary star might be the presence of a large amount of very dense gas ($n_{\text{H}_2} > 10^5 \text{ cm}^{-3}$ versus $n_{\text{H}_2} > 10^3 \text{ cm}^{-3}$), all other conditions being equal.

The star formation efficiency in the central $0.46 \times 0.46 \text{ pc}$ region of this cluster is nearly 20%. We still do not understand why most of the available gas is not being used up in the star formation process.

We would like to thank our scientific support person, Ron Probst, of KPNO, for his help in familiarizing us with data taking at the 1.3 m telescope. M. B. wishes to acknowledge the software support provided by Jeanette Barnes of NOAO and the timely delivery of beautiful photographs of the final mosaiced images by R. Seaman, also of NOAO. We thank R. Elson, C. J. Lada, P. C. Myers, and S. Stahler for helpful discussions. J. S. appreciates comparison of derived instrumental colors with the data of J. Salzer, D. Silva, and G. Bothun. M. B. was supported by a President's Fellowship from the University of California during the course of this work.

REFERENCES

- André, P., Montmerle, T., & Feigelson, E. D. 1987, *AJ*, 93, 1182
- André, P., Montmerle, T., Feigelson, E. D., Stine, P. C., & Klein, K. L. 1988, *ApJ*, 335, 940
- Barsony, M. 1989, Ph.D. thesis, California Institute of Technology
- Barsony, M., Burton, M. G., Russell, A. P. G., Carlstrom, J. E., & Garden, R. 1989, *ApJ*, 346, L93
- Barsony, M., Scoville, N. Z., Schombert, J. M., & Claussen, M. J. 1990, *ApJ*, 362, 674
- Becker, R. H., & White, R. L. 1988, *ApJ*, 324, 893
- Beichman, C., Myers, P. C., Emerson, J. P., Harris, S., Mathieu, R., Benson, P. J., & Jennings, R. E. 1986, *ApJ*, 307, 337
- Blaauw, A. 1964, *ARA&A*, 2, 213
- Christie, R. A., McCutcheon, W. H., & Chan, C. P. 1982, in *Regions of Recent Star Formation*, ed. R. S. Roger & P. E. Dewdney (Dordrecht: Reidel), 347
- Cohen, M., Biegging, J. H., & Schwartz, P. R. 1982, *ApJ*, 253, 707
- Elias, J. H., Frogel, J. A., Matthews, K., & Neugebauer, G. 1982, *AJ*, 87, 1029
- Fowler, A., et al. 1987, *Opt. Engineering*, 26, 232
- Herbig, G. H. 1971, *ApJ*, 169, 537
- Kenyon, S. J., Hartmann, L. W., Strom, K. M., & Strom, S. E. 1990, *AJ*, 99, 869
- Knapp, G. R., Kuiper, T. B. H., Knapp, S. L., & Brown, R. L. 1976, *ApJ*, 206, 443
- Lada, C. J., & Lada, E. A. 1991, in *The Formation and Evolution of Star Clusters*, ed. K. Janes (Astronomical Soc. Pacific Conf. Proc.) (Chelsea, MI: Astronomical Society of the Pacific)
- Lada, C. J., & Wilking, B. A. 1984, *ApJ*, 287, 610
- Lada, E. A., Bally, J., & Stark, A. A. 1991, *ApJ*, 368, 432
- Lada, E. A., DePoy, D. L., Evans, N. J., & Gatley, I. 1991, *ApJ*, 371, 171
- Larson, R. B. 1990, in *Physical Processes in Fragmentation and Star Formation*, ed. R. Capuzzo-Dolcetta, C. Chiosi, & A. Di Fazio (Dordrecht: Kluwer), 389
- Leous, J. A., Feigelson, E. D., André, Ph., & Montmerle, T. 1991, *ApJ*, in press
- Loren, R. B. 1989, *ApJ*, 338, 925
- McCaughrean, M. 1989, *S&T*, 77, 352
- Moneti, A., & Zinnecker, H. 1991, *A&A*, in press
- Montmerle, T., & André, Ph. 1988, in *Formation and Evolution of Low Mass Stars*, ed. A. K. Duprée & M. T. V. T. Lago (Dordrecht: Kluwer), 225
- . 1989, *Low-Mass Star Formation and Pre-Main Sequence Objects*, ed. B. Reipurth (Cambridge: ESO), 407
- Nelson, L. A., Rappaport, S. A., & Joss, P. C. 1986, *ApJ*, 311, 226
- Redman, R. O., Kuiper, T. B. H., Lorre, J. J., & Gunn, J. E. 1986, *ApJ*, 303, 30
- Salpeter, E. E. 1955, *ApJ*, 121, 161
- Shu, F. H. 1977, *ApJ*, 214, 488
- Stine, P. C., Feigelson, E. D., André, P., & Montmerle, T. 1988, *AJ*, 96, 1394
- Straw, S. M., Hyland, A. R., & McGregor, P. J. 1989, *ApJS*, 69, 99
- Stutzki, J., & Güsten, R. 1990, *ApJ*, 356, 513
- Wilking, B. A., & Lada, C. J. 1983, *ApJ*, 274, 698
- Wilking, B. A., Lada, C. J., & Young, E. T. 1989, *ApJ*, 340, 823
- Zinnecker, H. 1990, in *Physical Processes in Fragmentation and Star Formation*, ed. R. Capuzzo-Dolcetta, C. Chiosi, & A. Di Fazio (Dordrecht: Kluwer), 201